Direct thrust measurements of a 200 W Cylindrical Hall Thruster

IEPC-2024-747

Presented at the 38th International Electric Propulsion Conference, Toulouse, France
June 23-28, 2024

Tatiana Perrotin*, Pablo Fajardo† and Jaume Navarro-Cavallé‡
Department of Aerospace Engineering, Universidad Carlos III de Madrid, Leganés, Spain

George-Cristian Potrivitu§ and Jian Wei Mark Lim¶
Aliena Pte. Ltd., Singapore

A fully Cylindrical Hall Thruster is tested in the 200-400 W range of discharge power, coupled to a sub-ampere hollow cathode in self-sustained mode. The operating envelope covers voltages of 250-400 V and anode mass flow rates between 0.3 and 0.45 mg s^{-1}. Direct thrust measurements are performed with a hanging pendulum thrust balance. A maximum thrust of 7 mN is reached at 0.45 mg s^{-1} and 380 W of discharge power, corresponding to a thrust efficiency of 11.7% and anode efficiency of 13.8%. Ion current density measurements are used to estimate partial efficiencies and identify important loss mechanisms. High propellant utilization values are observed with a strong dependence on the propellant flow rate. The beam divergence efficiency and current utilization are both below 50%.

I. Introduction

The current needs of the space industry involve the use of efficient, compact, and affordable low-power propulsion systems with a large thrust-to-power ratio, to perform maneuvers such as orbit transfer, de-orbiting, and drag compensation within the limited time frames of short missions. Hall Thrusters (HT) are good candidates as they provide more thrust than other types of thrusters with comparable inputs and can be scaled to a wide range of operating powers. However, sub-kilowatt-class HTs require development to reach efficiencies and lifetimes as large as high-power HTs that benefit from several decades of research and flight heritage.[1]

Cylindrical Hall Thrusters (CHT) have the same operating principle as traditional annular HTs but feature a partially or fully cylindrical discharge chamber, and therefore a magnetic field with a significant axial component. This design was first investigated as a way of increasing the volume-to-surface ratio to avoid power losses and erosion of the inner ceramic wall while simplifying the mechanical design.[2] However, the alteration of the magnetic topology affects the dynamics of the plasma in the channel and plume, so, the behavior of the CHT must be further studied to optimize the device by understanding the phenomena occurring in the discharge. In addition, HTs require a hollow cathode (HC) for plasma generation and beam neutralization, but downscaling the cathode to be reliable while providing a low electron current with minimal electrical power and propellant consumption is challenging.

This work presents direct thrust measurements of a CHT designed to operate in the 100-300 W range. The thruster is coupled for the first time with a MUlti-Stage Ignition Compact (MUSIC) 1 A-class hollow cathode manufactured by Aliena Pte Ltd. The characterization covers a matrix of anode propellant mass flow rates and discharge voltages, and associates the measured thrust to the ion current density scans of

*Ph.D. student, tperroti@pa.uc3m.es.
†Professor, pfajardo@ing.uc3m.es.
‡Associate Professor, janavarr@ing.uc3m.es.
§Chief Technology Officer and Co-founder, georgepotrivitu@aliena.sg.
¶Chief Executive Officer and Co-founder, marklim@aliena.sg.

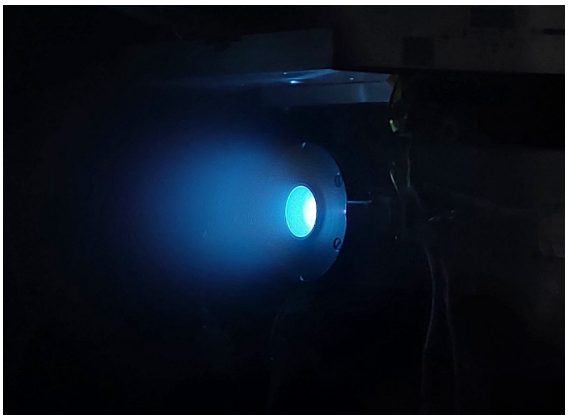

Figure 1: Picture of the CHT, mounted on the thrust balance, firing with xenon. The HC is visible on the right-hand side, in the foreground.

the plasma plume obtained with electrostatic probes. Those diagnostics provide information about the total thrust efficiency and partial efficiencies, allowing for the identification of the main loss mechanisms in this CHT-HC system. The measurements also serve the purpose of providing experimental data on the MUSIC HC operation and assessing its suitability for this thruster.

Existing published research has reported direct thrust measurements associated with partial efficiencies estimations using similar electrostatic probes, with relatively comparable CHT.[3–11] These publications cover a variety of CHT dimensions and operating ranges, but they are selected as the majority focuses on fully cylindrical channels, with direct magnetic fields, discharge voltages of 150-350 V, anode propellant flow rates of 0.3-1 mg s^{-1}, discharge powers of 60-450 W, and operation with a hollow cathode. Measured thrust levels range from $\sim$ 1.6 to 13 mN, and anode efficiencies range from $\sim$ 4 to 33%. Noticeable and recurring differences with the present work lie in the larger cathode mass flow rate employed ($\geq$ 1 mg s^{-1} in all other referenced work), the use of keeper power for most of the measurements, and the often lower discharge current. When partial efficiencies are estimated from probe measurements, they show generally similar or larger current utilization efficiencies than the ones presented in this work, and propellant utilization efficiencies above unity without accounting for the cathode flow.

This work constitutes the first operation of this CHT with a sub-amp hollow cathode, and the first direct thrust measurements of this prototype. Section II presents the experimental set-up used in this campaign. The thruster and cathode under test are described more thoroughly in paragraph II.A, while the measurement environment, tools, and procedures are introduced in paragraphs II.B and II.C. The results obtained are summarized in section III which presents the CHT-HC operating envelope in paragraph III.A, with details about the HC operation in paragraph III.B, the direct thrust measurements in paragraph III.C, and the plasma properties and performance assessed from the probe measurements in paragraphs III.D. Finally, section IV gathers the main conclusions and the future work.

II. Experimental set-up

A. Thruster and cathode

The CHT discharge chamber is made of boron-nitride. It is fully cylindrical, 26 mm in diameter, and 22 mm long (Fig. 1). The magnetic field is generated by two electro-magnets (C_1 and C_2) polarized in the same direction (co-current), and it is shaped by a high-permeability soft iron casing and central magnetic pole. The electromagnets are powered by two RS-Pro IPS3610D DC power supplies at $I_{C_1} = 1$ and $I_{C_2} = 1.7$ A. An annular copper anode, which also serves as the propellant injector, is placed at the outermost diameter of the channel upstream wall (Fig. 2 and 3). The design features of this device, including the magnetic topology, have been described more thoroughly in previous communications reporting studies with a variety of methods such as: numerical simulations of the internal and near-field CHT discharge,[12] two-dimensional mapping of the far-field plume with electrostatic plasma diagnostics,[13,14] and Laser-Induced Fluorescence spectroscopy measurements of the ions and atoms velocity in the internal and near-field plasma.[15] In these

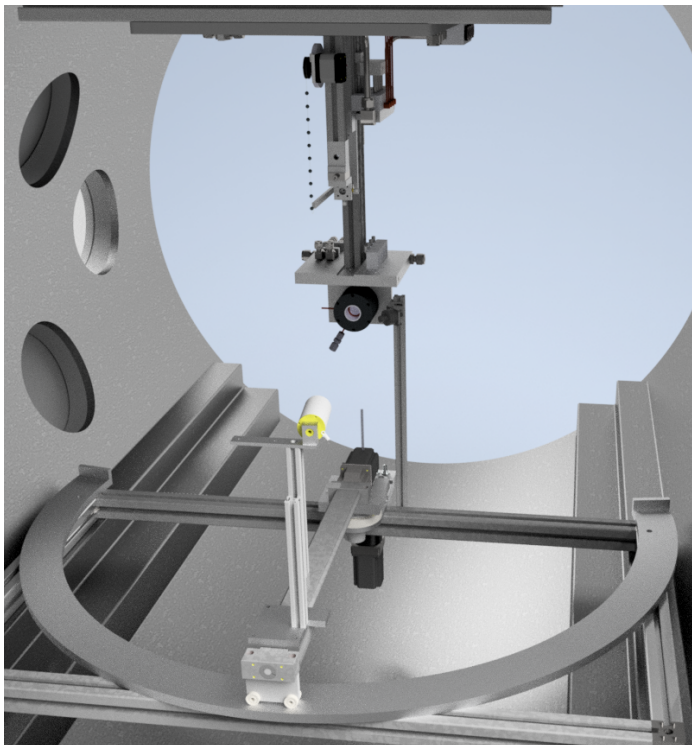

Figure 2: CAD assembly displaying the vacuum chamber with the thruster mounted on the thrust balance, the hollow cathode mounted on a vertical arm, and the Faraday cup mounted on the polar probe positioning system.

previous experimental studies, this CHT was coupled with a MIREA type 5 A-class LaB_6 pellet cathode.[16] In the current work, the MUSIC 1 A-class HC developed by Aliena Pte. Ltd. is used instead (Fig. 2). Further details about this device can be found in the work of Potrivitu et al.[17] This compact hollow cathode was optimized to be coupled with Aliena's 100 W-class Hall thruster, and it is therefore sized to provide emission currents between 0.1 and 1.2 A. In this work, the cathode is operated at the higher end of this range. When the measurements are performed, the HC is always operating in self-sustained mode, without heater or keeper power.

The HC is positioned in such a way that the keeper orifice is 55 mm aside from the thruster axis and 30 mm downstream of the exit plane, with the cathode axis forming a 45 ° angle with the thruster axis (Fig. 3). To ensure mechanical decoupling between the CHT and the HC assembly (wiring, tubing, etc.), the latter is mounted on its own separate structure. Consequently, any thrust produced by the cathode is not measured, but it is safe to assume it is negligible. This decoupling also allows for minimizing the conductive heat transfer between the two devices. The cathode assembly is kept electrically floating and the potential of the cathode (emitter) with respect to the grounded vacuum chamber is measured, it is later on referred to as the Cathode Reference Potential (CRP). The heater circuit, keeper and anode discharges are controlled with three DC power supplies (BK Precision 9117, Fug MCP 2800-2000 and BK Precision PV60085MR, respectively). Two sheathed K-type thermocouples are placed on the gas pipe and on the base of the cathode, respectively, to track the cathode thermal behavior along the tests. The cathode and anode are both fed with xenon propellant using two mass flow controllers calibrated for this gas (Mks MF-1 and Bronkhorst EL-FLOW select, respectively). The propellant mass flow rate injected through the cathode is $\dot{m}_c = 0.08$ mg s^{-1} for all the measurements presented in this work.

B. Vacuum facility

The tests are performed in the laboratory of the EP2 research group (UC3M, Madrid, Spain) which is equipped with a 3.5 m long, 1.5 m diameter cylindrical vacuum chamber made of non-magnetic stainless steel. The primary vacuum is achieved by means of a Leyvac LV80 dry mechanical pump (pumping

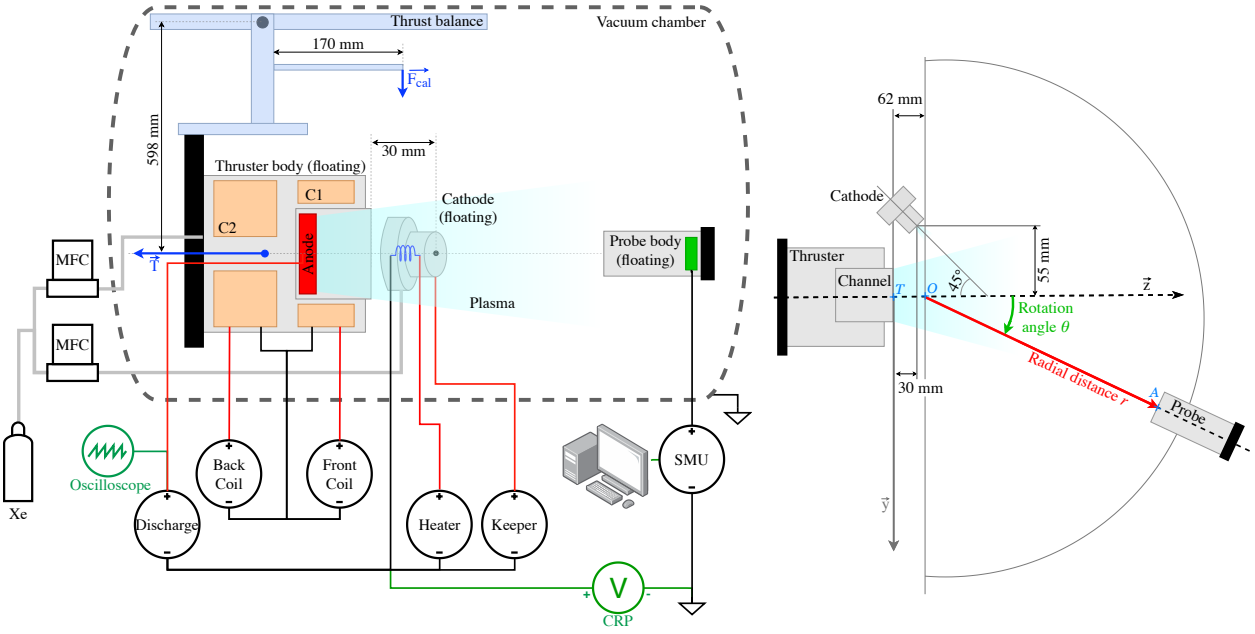

Figure 3: Schematic of the electric circuit, fluid, and mechanical circuit, including the relative positions of the thruster, thrust balance, cathode, and probes, viewed from the side (left) and from the top (right).

speed ~ 80 m^3 h^{-1}) and the pressure is brought down to $\sim 3 \times 10^{-7}$ mbar in dry conditions, with two Leybold MAGW2.200iP turbo-molecular pumps (each with a pumping speed of 2000 l s^{-1}) and two Leybold CoolPower 140 T-V cryogenic panels. The maximum total xenon mass flow rate during measurements is 0.53 mg s^{-1} (0.08 and 0.45 mg s^{-1} through the cathode and anode, respectively), under this load, the corresponding maximum pressure is $\sim 1.2 \times 10^{-5}$ mbar. The chamber is electrically grounded.

C. Diagnostics

1. *Plasma probes*

In order to better identify the specific processes responsible for efficiency losses in the thruster, diagnostics are used to measure a set of plasma properties.

The temporal behavior of the discharge current is recorded using an AC/DC Micsig CP2100A clamp current probe, the data is acquired with a Keysight InfiniVision MSO-X 3104A oscilloscope. The probe is placed on the atmospheric side of the cathode-anode circuit (Fig. 3).

The ion current density (j_i) in the plume is measured using a Faraday Cup (FC). The probe is composed of an electrically floating graphite split collimator with a 10 mm-diameter aperture. The aluminum collector is constituted of two elements: a 40 mm-long lateral cylindrical one and a conical one at the downstream end of the cup. The probe geometry is meant to reduce measurement errors potentially introduced by phenomena such as internal ionization, Secondary Electron Emission (SEE), and ion trajectory. Information related to the FC can be found in the work of Inchingolo et al.[18] The FC collector is electrically biased to -100 V with respect to the ground using a Keysight B2901A Source/Measure Unit (SMU), which measures the collected current (Fig. 3). This voltage is selected by performing a voltage sweep at various angles in the plume to ensure ion current saturation.

The FC is mounted on a polar probe positioning system that allows for displacement in the radial (r) and polar (θ) directions (Fig. 2 and 3). The center of rotation $\mathcal{O}$ of the arm is aligned with the thruster axis and is offset by 62 mm downstream from the thruster exit plane ($\mathcal{T}$) because of set-up constraints. The probe always points toward $\mathcal{O}$ and the distance between the probe aperture ($\mathcal{A}$) and $\mathcal{O}$ is $r = 451$ mm (Fig. 3). The beam current (I_{ib}) is estimated by integrating the current density over the hemisphere of radius 451 mm, under the assumptions of singly-charges ions, conical expansion, and axisymmetry of the beam, while taking the average of j_i at positive and negative angles.[14,19] This method slightly underestimates the

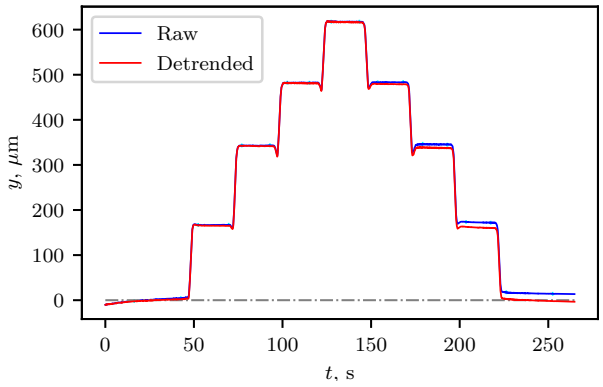

(a) Pendulum amplified displacement response throughout the calibration process: loading/unloading sequence of 4 calibrated weights. The detrended curve corrects for the average thermal drift.

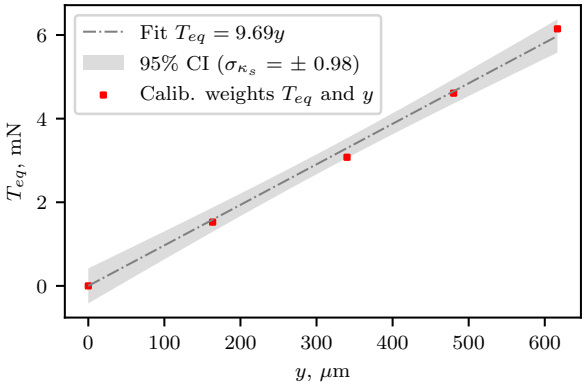

(b) Estimation of the balance stiffness, or calibration coefficient, κ_s, from the displacement due to each weight in Fig. 4a. It is the slope of the linear fit $y - T_{eq}$. The uncertainty on κ_s (σ_{κ_s}) is estimated from the standard deviation of the slope with a 95% confidence interval (CI).

Figure 4: Example of typical thrust balance calibration curves

real total current, mainly because of the lack of measurement of j_i at the outermost angles, from $\sim \pm 81$ to ± 90 °, which is considered small since $j_i(\theta = \pm 81\ ^\circ) \ll j_i(\theta = 0\ ^\circ)$, and because of the aperture view factor, which is also negligible since it decreases the collection area by $\leq 1\%$. The partial efficiencies deduced from I_{ib} are the current utilization (η_{cur}):

$$\eta_{cur} = I_{ib}/I_a, \tag{1}$$

where I_a is the anode current; the propellant utilization (η_u):

$$\eta_u = \frac{I_{ib} m_i}{q(\dot{m}_a + \dot{m}_c)}, \tag{2}$$

which assumes the presence of only singly-charged ions, $\dot{m}_a$ is the anode mass flow rate, m_i is the xenon ion mass, and q is the electron charge; and the divergence efficiency (η_{div}):

$$\eta_{div} = (I_{iz}/I_{ib})^2, \tag{3}$$

being I_{iz} the axial ion current. Further details regarding the assumptions, method, and calculation of intermediate variables can be found in Ref. 14.

Some properties such as the plasma potential (ϕ), plasma density (n), and electron temperature (T_e) are measured in the far-plume, on the thruster axis, using a cylindrical Langmuir Probe (LP). The probe axis is aligned with the thruster axis, and it is biased electrically using a Keithley 6517B electrometer which measures the collected current. The LP employed in this work has a 0.254 mm-diameter, 7 mm-long tungsten tip. It has internal electronic components and a secondary electrode exposed to the plasma for RF compensation, but this has no effect on the measurements presented here. This is verified by comparison with a traditional LP during the same campaign. The magnitudes presented hereafter are obtained from the LP current-voltage curves according to the method proposed by Lobbia and Beal[20] and detailed in previous work.[14]

2. *Thrust balance*

The direct thrust measurements presented in section III.C are performed using a mechanically amplified thrust balance (TB) designed for electric thrusters with thrust levels in the order of the milli-newton. The TB is visible in the upper half of Fig. 2. The design is based on the Variable Amplitude Hanging Pendulum with Extended Range (VAHPER) introduced by Polzin et al.[21] A detailed description of this implementation

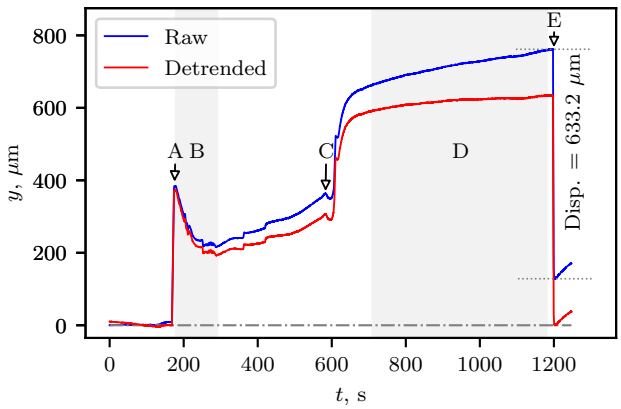

Figure 5: Example of typical measurement displaying the evolution of the thrust balance amplified displacement over time, from the thruster ignition to shutdown (anode voltage and flow rate). The TB displacement when switching off the thruster is 633 μm at $\dot{m}_a = 0.4$ mg s^{-1} and $V_a = 350$ V

can be found in the work of Wijnen et al.[22,23] It is constituted of a main structure supporting a secondary horizontal arm coupled to the primary pendulum with a set of fixed and freely-moving pivots, permitting the mechanical amplification of the displacement. An Eddy current damping system damps the motion at the extremity of the secondary arm, where a confocal chromatic sensor measures the amplified displacement with a sampling frequency of 10 Hz. The electronics of the optical instrument are placed on the atmospheric side and the light signal is carried to/from the vacuum side through an optical fiber. The thruster is mounted onto the main vertical arm thanks to a plate, at its bottom end. This plate, which can be actively cooled, serves as mechanical, electrical and fluid interface between the thruster and the fixed platform of the balance that is anchored to the vacuum chamber. The pipes and cables connecting the movable and fixed parts of the balance induce a low stiffness. The optical signal is acquired with the commercial STIL CCS-Prima software of the optical sensor, which provides directly the measured displacement.

Since the dynamic response of the TB pendulum depends on the thruster mass and the testing conditions, it is equipped with a calibration system that allows for measuring the stiffness of the system remotely, while in vacuum. This system is described in the work of Inchingolo et al.[24] Essentially, a set of four ~ 0.55 g weights is added sequentially to an horizontal arm of length $L_{cal} = 170$ mm protruding from the main pendulum (Fig. 2 and 3). Each weight added to the arm contributes to the increase of the known calibration force F_{cal} applied, which produces a torque on the vertical pendulum, as the thrust does. This equivalent thrust (T_{eq}) only depends on the lever distances of the applied forces (L_{cal} for F_{cal} and $L_T = 598$ mm for T_{eq}):

$$T_{eq} = F_{cal} \frac{L_{cal}}{L_T}. \tag{4}$$

Note that L_T is the distance from the pivot to the thrust vector, assuming it is located at the center of the CHT, pointing along its axis. The displacement (y) generated by each applied weight (Fig. 4a) is associated with the calibration force/equivalent thrust through the calibration factor $F_{cal} = k_{cal} y$. This relation is assumed linear over the small range of forces considered, therefore $\kappa_s = L_{cal} L_T^{-1} k_{cal}$ is determined with a linear fit, as shown in Fig. 4b. Then, the following equation can be used to compute the thrust for a measured or known displacement y:

$$T_{eq} = \kappa_s y. \tag{5}$$

3. Measurement procedure

The measurement and calibration sequence is of utmost importance to ensure reliability of the data, therefore a number of constraints must be taken into account. The measurement itself has to be isolated from any phenomena causing displacements of the highly sensitive TB. With this intent, the cathode is mounted on a separate stand, entirely decoupled from the TB, so that its operation does not displace the TB. This is verified with tests. The CHT coils are not switched on/off during acquisition to avoid any interaction of the magnetic field with other magnetic equipment in the facility, which are kept static too. It is verified that

applying a voltage bias to the anode (in the absence of plasma) does not cause any displacement. Special care is taken in the set-up and procedure to minimize as much as possible the measurement errors arising from transients (mechanical, plasma, fluid, thermal, etc.) and general variations of temperature inducing thermal expansion of the thruster and/or the TB and therefore changes of geometry and stiffness.

For each thrust measurement, the cathode is heated up until keeper ignition, then a first TB calibration is performed (e.g. Fig. 4a). After this, the anode discharge is ignited with only one electromagnet (C_1). All the parameters are gradually adjusted to get to the target operating point: I_{C_1}, I_{C_2}, $\dot{m}_c$, the cathode heater current (I_h) and keeper current (I_k), the anode voltage (V_a) and mass flow rate ($\dot{m}_a$), and a few minutes are left for the anode discharge current (I_a) to settle. In a typical TB displacement acquisition, these steps show clearly as variations in thrust (Fig. 5, $\sim$ 175 to $\sim$ 620 s) followed by a roughly linear region due to the plateauing thrust (target operating point reached) and a thermal drift. The probe (FC, LP) measurements are done in this interval. This drift is usually not really linear over the whole firing time, or even before, or after, because the power dissipation varies and the thermal loads induce mechanical deformation of the system. The thrust is measured as the anode power supply is switched off and $\dot{m}_a$ is set to zero, simultaneously (Fig. 5). Only the cathode propellant flow rate and the CHT magnetic field remain, as previously stated, they do not disrupt the displacement step. These behaviors are identified with letters in Fig. 5, as follows: (A) thruster ignition ($\sim$ 175 s), (B) discharge current dropping due to cathode cooling from ignition ($\sim$ 180-300 s), (B) to (C) discharge progressively switching to voltage saturation and steady discharge current, (C) discharge voltage set to target operating point ($\sim$ 620 s), (D) discharge reaching steady current ($I_a \sim 0.907$ A), (E) thrust measured at the moment the anode voltage and mass flow rate are switched off simultaneously ($\sim$ 1200 s). The detrended curve is the subtraction of the raw curve and the global linear thermal drift interpolated between ignition and shutdown.

The rapid increase of y after that point is attributed to the fast cooling of the balance in the sudden absence of heating from the plasma. The TB pendulum settling time from the thrust step is significantly faster than this phenomenon.[22] The slowest transient is the one of $\dot{m}_a$, but it is overlooked since its contribution to y is minimal and would show an opposite variation of y. Soon after the acquisition, the coils and cathode flow are turned off, and a new calibration is executed to characterize κ_s in thermal conditions as close as possible to the ones during thruster operation. This value of κ_s from the second calibration is the one used in Eq. 5 to evaluate T. The thrust efficiency (η_T) is then computed with the relation:

$$\eta_T = \frac{T^2}{2(\dot{m}_a + \dot{m}_c)P_a}. \tag{6}$$

III. Experimental results

A. Operating envelope

The CHT characterized in this work is coupled for the first time with a hollow cathode capable of self-sustained operation at a low current and low propellant flow rate ($\dot{m}_c \ll \dot{m}_a$). After finding a suitable $\dot{m}_c$ for stable operation of the voltage-saturated discharge, the achievable range of this CHT-HC system is investigated by varying the discharge voltage (cathode to anode) and the anode flow rate, $\dot{m}_a$ and V_a, over the ranges 0.30 to 0.45 mg s^{-1} and 250 to 400 V, respectively.

Table 1 shows, for each test point, the average discharge current $\langle I_a \rangle$, average discharge power $\langle P_a \rangle$, and average keeper floating voltage $\langle V_k \rangle$ (with respect to the cathode). The magnitudes are averaged over at least two repetitions of the same input conditions (V_a and $\dot{m}_a$). Spontaneous and seemingly random variation of the discharge current for the same V_a and $\dot{m}_a$ from one execution to another resulted in the dispersion of I_a given in Table 1. Therefore, information about the deviation from the average is also provided. The deviation of P_a ensues from the one of I_a. This non-monotonic variation of I_a occurred for all test conditions, it could be attributed to the combination of multiple phenomena such as material deposition on the ceramic walls and anode (which is observed), erosion of thruster parts, change of surface state or cleaning of the cathode emitter, or electromagnet degradation. The measurements are done once the variation of the power supply reading of the discharge current (time average) is smaller than 10 mA over several minutes, to avoid major ignition transients.

Lower mass flow rates are explored but not reported as they translate into a gradual drop of I_a until the discharge extinguishes. Lower voltages lead to a very unstable discharge behavior and are therefore excluded from the study. On the higher end of the range, a hard limit is set to $I_a = 1.2$ A as per the recommendations

Table 1: Average discharge current ($\langle I_a \rangle$), average discharge power ($\langle P_a \rangle$), and average keeper floating potential ($\langle V_k \rangle$) for a range of anode mass flow rates ($\dot{m}_a$), and anode voltages V_a. The average is done over at least two instances of the same operating conditions. The maximum deviation from the average value is given.

			V_d (V)			
			250	300	350	400
$\dot{m}_a$ (mg s^{-1})	0.30	$\langle I_a \rangle$ (A)	0.882 ± 0.043	0.734 ± 0.006	0.752 ± 0.022	0.742 ± 0.008
		$\langle P_a \rangle$ (W)	220 ± 10	220 ± 1	263 ± 7	297 ± 3
		$\langle V_k \rangle$ (V)	19.8 ± 0.1	22.1 ± 0.95	21.7 ± 0.33	21.4 ± 0.6
	0.35	$\langle I_a \rangle$ (A)	0.942 ± 0.006	0.853 ± 0.054	0.827 ± 0.021	0.878 ± 0.062
		$\langle P_a \rangle$ (W)	235 ± 1	255 ± 16	289 ± 7	351 ± 25
		$\langle V_k \rangle$ (V)	16.8 ± 0.1	20.9 ± 0.95	17.4 ± 0.95	17.6 ± 1.9
	0.40	$\langle I_a \rangle$ (A)	1.083 ± 0.107	1.005 ± 0.050	0.946 ± 0.074	1.000 ± 0.070
		$\langle P_a \rangle$ (W)	270 ± 26	301 ± 14	331 ± 25	399 ± 28
		$\langle V_k \rangle$ (V)	15.6 ± 0.1	18.6 ± 1.45	18.4 ± 2.8	13.7 ± 3.2
	0.45	$\langle I_a \rangle$ (A)		1.060 ± 0.040	1.085 ± 0.040	
		$\langle P_a \rangle$ (W)		318 ± 12	379 ± 13	
		$\langle V_k \rangle$ (V)		16.8 ± 0.2	15.8 ± 0.7	

from the HC manufacturer. Combining large mass flow rates and voltages results in fast heating of the thruster chamber, anode, and coil C_1 due to the large discharge power and is therefore avoided.

Table 1 shows a strong dependence of I_a on $\dot{m}_a$, which is a direct consequence of the plasma production enhanced by a larger neutral density. For each mass flow rate, the average discharge current is the largest at the lowest voltage and reaches a minimum at an intermediate voltage. This observation differs from previous characterizations of the same CHT with a different neutralizer.[14] The mechanism that causes this minimum in the discharge current has not been identified.

B. Hollow cathode operation

Specific attention is given to the cathode operation in this campaign since it is used for an extended duration close to its higher current limit, and systematically self-heated. The HC is fed with a propellant flow rate slightly below the expected one from diode characterization with a simple anode. Despite the low $\dot{m}_c$ of the MUSIC HC, the CHT discharge sets at currents about twice as large as in previous tests with other HC.[14,15] This indicates that the cathode geometry and required amount of propellant can strongly affect the properties of the cathode plasma plume, such as the extracted electron current, and possibly other magnitudes (density, temperature, etc.). This, in turn, affects the thruster-cathode coupling through the discharge current, the coupling potential, and the ion production which depends on the electron temperature. It is also possible that the facility influences the plasma properties and discharge current.

Keeper ignition is achieved with a 300 V bias and a heater power $P_h \sim 42 - 55$ W, after a $\sim 7 - 8$ min current ramp-up. The cathode is ignited over 84 times along the campaign, accumulating ~ 30 h of operation. The repeatability of the heater current-voltage characteristic is preserved (Fig. 6a).
Given the large discharge current extracted from the HC with this CHT, and the general test set-up, the temperatures reached are also more elevated than in typical operation of the MUSIC HC. The monitored temperatures of the base and gas inlet are presented in Fig. 6b, in which important events throughout the test sequence are indicated. The HC temperature rises at a faster pace once the thruster is ignited because of the large initial current, and then cools down as P_h and P_k are switched off and I_a settles.

The keeper floating voltage with respect to the cathode is given in Table 1 for each operating point. It increases as $\dot{m}_c$ goes down, which is representative of the cathode itself floating further from the ground potential. This is due to increased plasma sheath potential at the cathode emitter, at low cathode flow rates, and therefore low cathode internal pressure. The value of V_k does not change significantly with V_a, but it does sufficiently to display a maximum at $V_a = 300$ V for all $\dot{m}_c$.

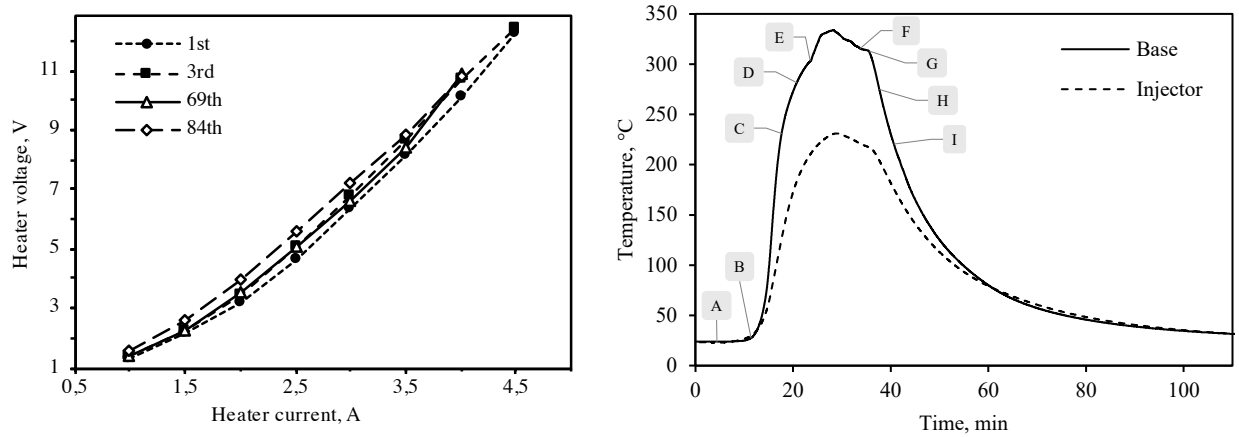

Figure 6: Measured cathode properties: (a) Evolution of the cathode heater I-V curve with the number of ignitions, and (b)thermocouples readings at the cathode base (solid line) and gas pipe (dashed line) along time during the measurement sequence. The labels indicate : (A) the beginning of the cathode heating, (B) the keeper ignition, (C), the beginning of the first TB calibration, (D) the end of the first TB calibration, (E) the stabilization of the thruster, (F) the ending of the FC scan, (G) the extinguishing of the thruster, (H) the beginning of the second calibration, (I) the end of the second calibration.

C. Direct thrust measurements

For each one of the operating points presented in Table 1, the thrust is measured following the procedure described in section II; the results are presented in Fig. 7.

Each measurement is performed at least twice, and for some points multiple times (up to 24, in the case $\dot{m}_a = 0.4$ mg s^{-1} and $V_a = 350$ V). The various executions are done in different, non-consecutive ignitions. In Fig. 7, the markers indicate the average thrust $\langle T \rangle$ and average thrust efficiency $\langle \eta_T \rangle$ (from Eq. 6) over all the executions of each operating point, and the error bars indicate the dispersion range.

The thrust is strongly dependent on both $\dot{m}_a$ and V_a. It increases more or less linearly with $\dot{m}_a$ for a given V_a. The thrust can be expected to scale as $T \propto \dot{m}_a \sqrt{V_a}$. Note that this approximation is not exact since it relies on a number of assumptions such as the negligible fraction and acceleration of non-ionized propellant, a high (almost ideal) voltage utilization efficiency, the presence of only mono-energetic singly-charged ions, etc. The data follows this law rather well for $\dot{m}_a \geq 0.35$ mg s^{-1}. At $\dot{m}_a = 0.30$ mg s^{-1}, however, the evolution of the thrust is not so straightforward and seems closer to a parabolic function of V_a. This suggests that at this low mass flow rate, more intricate changes occur in the internal discharge, and the effective potential drop for ion acceleration does not simply scale directly with $\sqrt{V_a}$.

Figure 5 shows that the efficiency is more sensitive to V_a than to $\dot{m}_a$ in the observed range. It increases very mildly with $\dot{m}_a$. As the anode bias rises, η_T does as well. At 0.3 and 0.4 mg s^{-1} it reaches a maximum around $V_a = 350$ V. However, it increases unbounded at 0.35 mg s^{-1}, while at 0.45 mg s^{-1}, the data available is scarce. Thus, any robust conclusions cannot be drawn in this regard. The consequent variation of η_T with P_a (not represented) is similar to the trend observed in the low-power fully Cylindrical Hall Thruster characterized by Shirasaki and Tahara,[7] with a saturation of η_T occurring at a larger value and power when $\dot{m}_a$ increases. The efficiencies presented here are overall a few percent below the values reported in the research mentioned in section I.[3–11] However, the cited literature usually provides values of anode efficiency rather than thrust efficiency, therefore overlooking the $\dot{m}_c$ and any heater or keeper power, which in some cases it is up to 40% of the discharge power P_a.

To provide some insight into the various contributions to the thrust,[24] the cold gas thrust is measured by feeding propellant to the anode, in vacuum conditions, while the thruster and cathode are switched off and cold. The acquired data are depicted in Fig. 8 for various $\dot{m}_a$. The expected linear relation between T and $\dot{m}_a$ is highlighted with a curve fit. The xenon cold thrust is ~ 198 μN/(mg s^{-1}). In operation, a large fraction of the propellant is ionized, so the ejected neutral mass flow rate is smaller than at the injection.

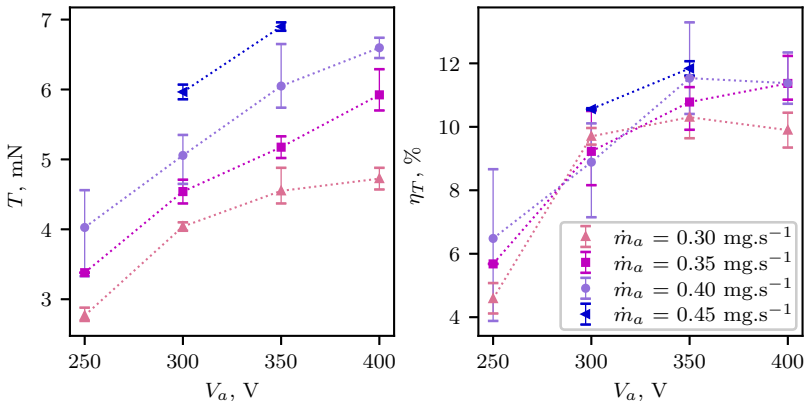

Figure 7: (Left) Average thrust $\langle T \rangle$ and (right) thrust efficiency $\langle \eta_T \rangle$ as a function of the discharge voltage V_a. The error bars indicate the dispersion of the data over multiple executions of the measurements at the same V_a and $\dot{m}_a$. The thrust efficiency includes the cathode propellant consumption.

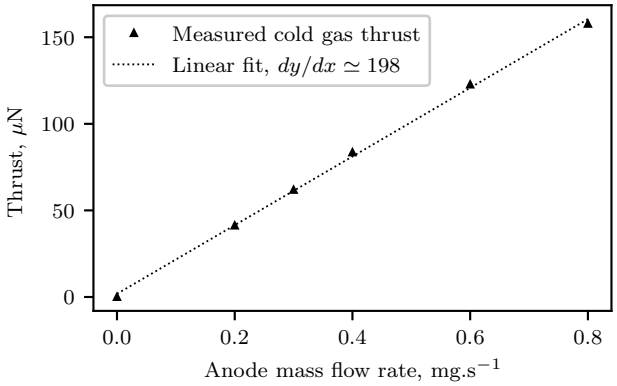

Figure 8: Linear dependence of the thrust on the anode propellant mass flow rate, in cold conditions.

Since the neutral gas velocity remains low even in operation, the measurements in Fig. 8 give a conservative estimate of the maximum possible neutral thrust.

D. Plasma properties measurements in the plume

1. Ion current density measurements

While direct thrust measurements provide objective information about the CHT-HC performance, other diagnostics are necessary to draw a complete picture of the specific mechanisms affecting the behavior of the thruster. Faraday cup measurements of the ion current density in the plume are done for this purpose. Polar scans of j_i in a plane of symmetry of the thruster are given in Fig. 9, for the matrix of operating points introduced in Table 1. Each column of subplots corresponds to a given discharge voltage (indicated above), and each row corresponds to an anode flow rate (indicated on the right-hand side).

The measurements are repeated two to four times, on different non-consecutive ignitions, that could correspond to different days (indicated in the legend as the number of days since day 0). In a similar manner as I_a, for the same inputs, j_i slightly increases and seems to reach some saturate. For instance, this can be observed for $\dot{m}_a = 0.4$ mg s^{-1} and $V_a = 350$ V in Fig. 9, where j_i drops between the first and second executions, and increases to an intermediate value in the third execution.

The profiles are composed of a broad single lobe, with some minor asymmetries. On the left-hand side, it

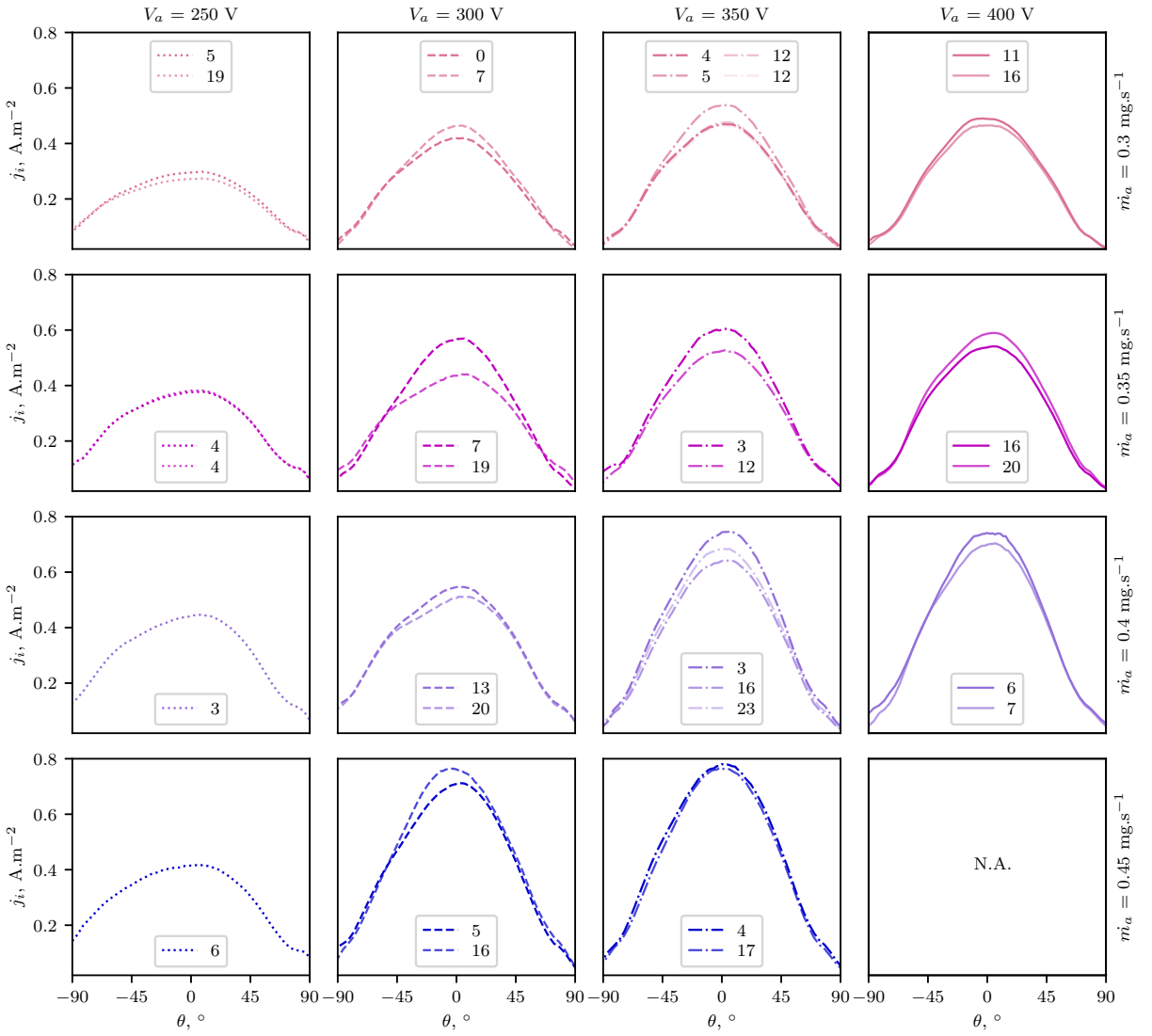

Figure 9: Faraday cup scans of the plume ion current density (j_i) for various values of V_a (indicated above) and $\dot{m}_a$ (indicated on the right), with a -100 V probe collector bias. The legends and curve opacity indicate the day (since day 0) on which each individual scan was performed (mostly on separate and non-consecutive firings).

shows a slightly larger j_i around -50 °. This side is the one where the cathode is located. Another possible source of asymmetry in the measurement plane is the non-homogeneity of the propellant injection, although the anode has an internal distributor with multiple orifices, this may be not sufficient to ensure uniform xenon injection into the discharge chamber.

Wide angles are nearly unaffected by the variation of the parameters, apart from a very slight increase of j_i as $\dot{m}_a$ increases. At narrow angles around the axis, the current density clearly changes with $\dot{m}_a$ and V_a. It is maximized for $\dot{m}_a = 0.45$ mg s^{-1} and $V_a = 350$ V, which corresponds to the largest η_T measured (Fig. 7). The evolution of the profile with V_a shows that, on average, j_i is the largest at 350 V. Increasing the anode flow rate likely enhances the plasma production and results in more current collected with the probe.

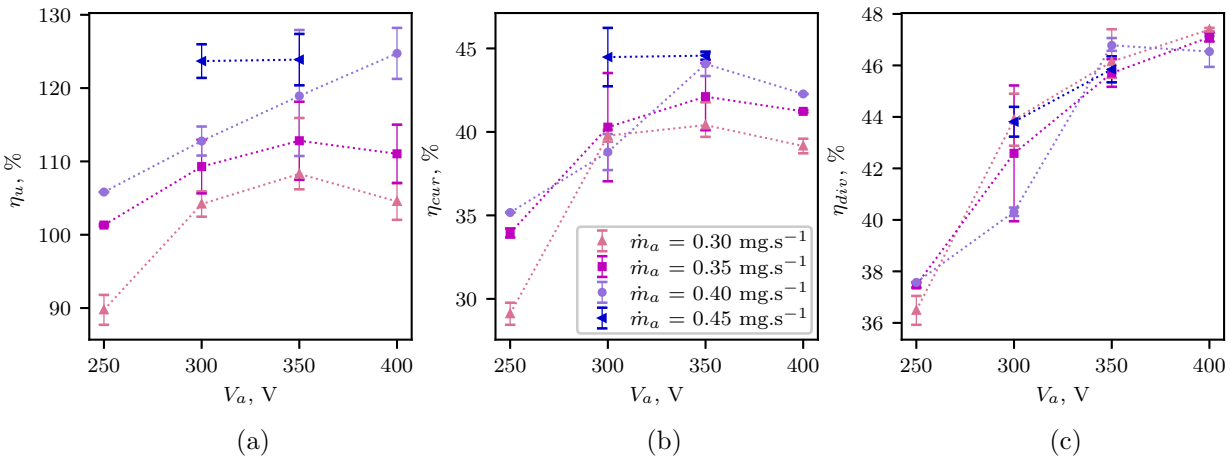

Figure 10: Evolution of the (a) propellant utilization efficiency η_u (using the total mass flow rate), (b) current utilization efficiency η_{cur} and (c) divergence efficiency η_{div} as a function of the discharge voltage V_a. The error bars indicate the dispersion of the data over multiple executions of the measurements at the same V_a and $\dot{m}_a$.

2. *Performance assessment from the ion current density*

As mentioned in section II, some performance metrics can be evaluated from the FC scans. Figure 10 a, b, and c depict the variation with V_a and $\dot{m}_a$ of the propellant utilization accounting for the total mass flow rate ($\dot{m}_a + \dot{m}_c$), the current utilization, and the divergence efficiency respectively.

In Fig. 10 a, it is clear that the propellant utilization increases significantly as $\dot{m}_a$ is ramped up from 0.3 to 0.45 mg s^{-1}, regardless of the voltage. The variation is in the order of 15 percentage points per 0.1 mg s^{-1}. As previously stated, it is the expected response to an increase of neutral density in the channel, and thus to a larger ionization collision rate.

The relation between η_u and V_a is less trivial: the utilization seems to increase up to a maximum at 350 V, for the lower mass flow rates, while it increases monotonically for 0.4 mg s^{-1} and does not vary for the largest $\dot{m}_a$. The range of V_a does not allow for determining if η_u reaches a maximum value for large $\dot{m}_a$.

It is worth noticing that η_u is largely above 100% for all test points but one, despite $\dot{m}_c$ being accounted for in Eq. 2, and the expected minor overestimation of I_{ib} due to the probe positioning system offset (section II). This is observed in most research on CHT and often attributed to the presence of important fractions of multiply-charged ions.[7–9, 25–27] Future characterization of this CHT with this cathode will include ExB probe measurements to quantify the ion populations, discriminating their charge and velocity. The confirmation of the existence of multiply-charged ions in this CHT-HC system would allow for identifying one of the phenomena causing a reduction of the thrust.[1]

The current utilization plotted in Fig. 10 b also generally rises with the mass flow rate in most cases, this dependence changes over the test envelope and is not clear at low voltages, but remains below ~ 6 percentage points per 0.1 mg s^{-1}. As $\dot{m}_a$ goes up, the larger neutral density allows for the generation of a larger plasma density and therefore an increased amount of electrons collected by the anode, however, the gain in ion beam current is more significant than the increase of electron current (estimated with the difference between I_d and I_{ib}), so η_{cur} increases with $\dot{m}_a$.

The electron current is particularly substantial at $V_a = 250$ V, with a very low utilization. As V_a takes greater values, η_{cur} takes a step of $\sim 6 - 11$ percentage points and reaches up about $35 - 40\%$ (depending on $\dot{m}_a$) around $V_a = 350$ V. Stepping V_a up from 250 to 300 V seems to induce a transition in the axial electron transport mechanisms. The trend of η_{cur} with V_a for this thruster compares well with existing CHT in literature,[5, 9, 10, 27] although η_{cur} typically increases more smoothly with V_a. The reported measurements cover a broad range of values which can be as low as $\sim 30\%$ and as high as $\sim 70\%$. This means that there is room for improvement of the electron transport suppression, which could be achieved by optimizing the magnetic topology and anode geometry, and potentially lead to global performance enhancement since this is a dominant efficiency loss mechanism.

Finally, the computed divergence efficiency is presented in Fig. 10c. Overall, η_{div} is low and constitutes

one of the main loss processes. A large divergence is a known drawback of most CHT,[9] it is expected to come from the non-negligible radial effects created by the peculiar magnetic topology, it is much more significant than in annular Hall thrusters with an almost fully radial magnetic field in the acceleration region.

The divergence is unaffected by $\dot{m}_a$ in the range of interest, but increasing V_a clearly improves the beam focusing. η_{div} seems to approach an asymptotic limit around 400 V, but the range of V_a should be extended to confirm this hypothesis.

3. Plasma potential, density, and electron temperature from Langmuir probe traces

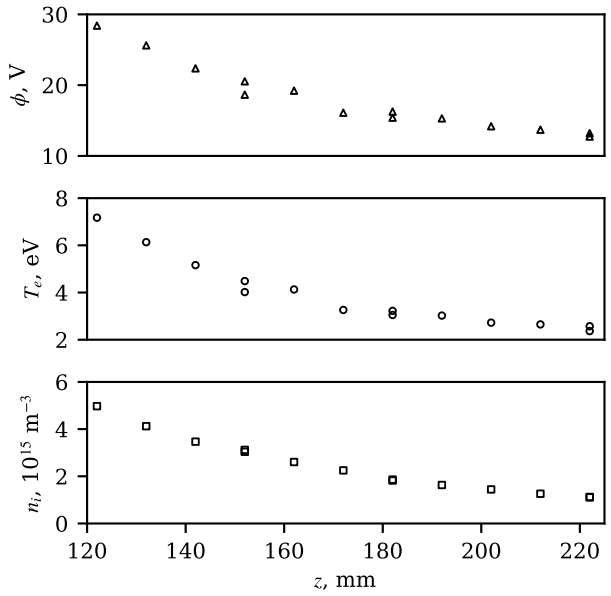

Figure 11: Plasma potential (ϕ), ion plasma density (n_i), and electron temperature (T_e) obtained from Langmuir Probe measurements on the thruster axis, for $V_a = 350$ V and $\dot{m}_a = 0.4$ mg s^{-1}. z is the distance from the thruster exit plane to the probe tip.

Langmuir Probe measurements are performed in the far plume of the CHT in the operating conditions $V_a = 350$ V and $\dot{m}_a = 0.4$ mg s^{-1}. The LP is displaced along the thruster axis over the range of distances $z \sim 12 - 22$ cm from the exit plane.

The monotonic decrease of the three parameters presented in Fig. 11 corresponds to the expected behavior.[9,14] The density, in the order of 10^{15} m^{-3}, is two to five times lower than previously observed in the same device when coupled to a very different hollow cathode (MIREA),[14] as mentioned in section II. While the $\dot{m}_a$ is larger in the present work, $\dot{m}_c$ is significantly lower, which might be correlated to this observation. This, as well as the large η_u reported earlier, will require further investigation of the presence of multiply-charged ions to ensure the validity of the analysis. Facility effects must also be considered as a possible factor in the differences in operation observed with the MIREA and MUSIC cathodes since the tests are performed in very different vacuum facilities.

The plasma potential and electron temperature are both much larger for the CHT coupled to the MUSIC HC, compared to those previous measurements. Note that V_a is 50 V larger in the present study. Indeed, ϕ drops from $\sim$ 30 to 12 V over the considered spatial range. It is up to 3 times larger than in Ref. 14 (despite a significantly more reasonable CRP) and suggests that the ion beam is not fully accelerated 22 cm downstream of the thruster exit, and a non-negligible fraction of V_a is likely not used for ion momentum generation. This hypothesis will be verified in the future with ion energy measurements. An important difference is that in this case, the CRP might not be the only significant source of voltage utilization loss, as it seemed to be in these previous measurements with a MIREA cathode. Other work on CHT identified that the cathode operation can have an important effect on the axial location of the acceleration region of the thruster and therefore on the thruster performance.[28] The electrons in this case reach temperatures up

to ~ 5 times larger than in Ref. 14, which could result from the very low $\dot{m}_c$ decreasing the collisionality and the electron cooling in the cathode plasma.

IV. Conclusions

The work presented here reports the performance characterization of a 200 W-class fully Cylindrical Hall thruster. It is the first experimental campaign that couples this prototype with the sub-ampere MUSIC hollow cathode from Aliena Pte. Ltd. The operating envelope of the CHT-HC system is explored by varying V_a from 250 to 400 V and $\dot{m}_a$ from 0.30 to 0.45 mg s^{-1}, while the HC functions in self-sustained operation. The discharge current lies between ~ 0.73 and 1.1 A. The thermal behavior of the HC is monitored along the tests and the health of the heater is verified with its electrical parameters over more than 80 cycles.

Direct thrust measurements are performed over a matrix of test points, leading to a maximum thrust of ~ 7 mN at $V_a = 350$ V and $\dot{m}_a = 0.45$ mg s^{-1}. Thrust efficiencies ranging from ~ 4 to 12% are reported. Both V_a and $\dot{m}_a$ contribute positively to the generation of thrust, and the efficiency is mainly affected by V_a, reaching a maximum around 350 V. The thrust produced by the neutral gas is measured in cold conditions and approaches 200 μN/(mg s^{-1}).

Scans of the ion current density in the plume are done with a Faraday cup and analyzed to extract partial efficiencies from the total ion current. Large propellant utilization values (> 1) are obtained and suggest the possibility of multiply-charged ions contributing to the measured current, as reported in most research on CHT. Values of current utilization and divergence efficiency below 50% are estimated, with a strong dependence on V_a and the apparent existence of an optimal voltage. These two efficiencies appear to highlight that some major drawbacks of this CHT are related to the wide beam angle and the excessive electron transport to the anode.

Plasma properties derived from Langmuir Probe measurements are provided on this axis for a selected operating point. The results present plasma potentials as large as 30 V at 12 cm from the thruster, indicating the possibility that the ion acceleration does not make efficient use of the whole potential drop available. Electron temperatures up to 7 eV and ion densities in the order of 10^{15} m^{-3} are measured and compared to available data from the plume of the same CHT coupled to a different HC.

This work is part of the ongoing characterization of this low-power CHT, and future experiments are planned with diagnostics such as a retarding potential analyzer and an ExB probe, to determine the ion velocity in the plume and assess the presence of multiply charged ions. This will allow for evaluating more accurately the various phenomena responsible for efficiency losses. Future work will also involve further characterization of the oscillatory behavior of the CHT-HC system and its effect on the discharge parameter.

Acknowledgments

This work has been supported by the project COMIT funded by the Spanish Government (grant PDC2021-120911-I00). The authors would like to thank Marco R. Inchingolo for sharing his knowledge of the thrust balance used in this work, and the team of Aliena Pte Ltd. for providing the hollow cathode used in this campaign and the associated support.

References

[1]D. M. Goebel and I. Katz, *Fundamentals of Electric Propulsion: Ion and Hall Thrusters*. john wiley & sons ed., 2008.

[2]Y. Raitses, L. A. Dorf, A. A. Litvak, and N. J. Fisch, "Plume reduction in segmented electrode Hall thruster," *Journal of Applied Physics*, vol. 88, pp. 1263–1270, Aug. 2000.

[3]M. Tisaev, B. Karadag, S. Masillo, and A. Lucca Fabris, "Performance and plasma diagnostics of the Air-breathing Microwave Plasma CAThode (AMPCAT) coupled to a cylindrical Hall thruster," *Journal of Applied Physics*, vol. 134, p. 193302, Nov. 2023.

[4]J. Lee, M. Seo, J. Seon, H. June Lee, and W. Choe, "Performance characteristics according to the channel length and magnetic fields of cylindrical Hall thrusters," *Applied Physics Letters*, vol. 99, p. 131505, Sept. 2011.

[5]Y. Gao, H. Liu, P. Hu, H. Huang, and D. Yu, "Effect of anode position on the performance characteristics of a low-power cylindrical Hall thruster," *Physics of Plasmas*, vol. 24, p. 063518, June 2017.

[6]Y. Gao, W. Wang, S. Xue, Y. Li, and G. Cai, "Influence of the upstream axial magnetic mirror field on the plume characteristics in the full cylindrical Hall thruster," *Acta Astronautica*, vol. 196, pp. 186–193, July 2022.

[7]A. Shirasaki and H. Tahara, "Operational characteristics and plasma measurements in cylindrical Hall thrusters," *Journal of Applied Physics*, vol. 101, p. 073307, Apr. 2007.

[8]K. D. Diamant, J. E. Pollard, Y. Raitses, and N. J. Fisch, "Ionization, Plume Properties, and Performance of Cylindrical Hall Thrusters," *IEEE Transactions on Plasma Science*, vol. 38, pp. 1052–1057, Apr. 2010.

[9]A. Smirnov, Y. Raitses, and N. J. Fisch, "Experimental and theoretical studies of cylindrical Hall thrusters," *Physics of Plasmas*, vol. 14, no. 5, p. 057106, 2006.

[10]S. Liang, H. Liu, and D. Yu, "Effect of permanent magnet configuration on discharge characteristics in cylindrical Hall thrusters," *Physics Letters A*, vol. 383, pp. 2272–2276, July 2019.

[11]S. Liang, H. Liu, and D. Yu, "Discharge channel configuration effect on the discharge characteristics of cylindrical Hall thrusters," *Physics Letters A*, vol. 395, p. 127221, Apr. 2021.

[12]T. Perrotin, A. Domínguez-Vázquez, J. Navarro-Cavallé, P. Fajardo, and E. Ahedo, "Design and Preliminary Study of a 200W Cylindrical Hall Thruster," in *Space Propulsion Conference*, (Estoril, Portugal), p. 11, 2021.

[13]T. Perrotin, A. E. Vinci, S. Mazouffre, J. Navarro-Cavallé, P. Fajardo, and E. Ahedo, "Characterization of a low-power Cylindrical Hall Thruster," in *37th International Electric Propulsion Conference*, (Massachusetts Institute of Technology, Cambridge, MA, USA), 2022-06-19/2022-06-23.

[14]T. Perrotin, A. E. Vinci, S. Mazouffre, P. Fajardo, E. Ahedo, and J. Navarro-Cavallé, "Far-field plume characterization of a low-power cylindrical Hall thruster," *Journal of Applied Physics*, vol. 136, p. 043304, July 2024.

[15]T. Perrotin, A. E. Vinci, S. Mazouffre, J. Navarro-Cavallé, P. Fajardo, and E. Ahedo, "Measurements of xenon ions and atoms velocity in cylindrical hall thruster with laser-induced fluorescence spectroscopy," in *10th EUCASS Conference*, (Lausanne, Switzerland, July 9–13), 2023.

[16]B. Vincent, S. Tsikata, G.-C. Potrivitu, L. Garrigues, G. Sary, and S. Mazouffre, "Electron properties of an emissive cathode: Analysis with incoherent thomson scattering, fluid simulations and Langmuir probe measurements," *Journal of Physics D: Applied Physics*, vol. 53, p. 415202, Oct. 2020.

[17]G.-C. Potrivitu, M. Laterza, S. Y. C. Gui, A. Chaudhary, M. Harriz, A. B. Ridzuan, C. Teo, and J. W. M. Lim, "Development of Hollow Cathodes for Hall Effect Thrusters at Aliena: Design, Ground Testing and Qualification for Space," in *9th Space Propulsion Conference*, (Glasgow, Scotland), 2024.

[18]M. Inchingolo and J. Navarro-Cavallé, "Faraday cup design for electrodeless plasma thrusters," in *10th EUCASS Conference*, (Lausanne, Switzerland, July 9–13), 2023.

[19]D. L. Brown, M. L. R. Walker, J. Szabo, W. Huang, and J. E. Foster, "Recommended Practice for Use of Faraday Probes in Electric Propulsion Testing," *Journal of Propulsion and Power*, vol. 33, pp. 582–613, May 2017.

[20]R. B. Lobbia and B. E. Beal, "Recommended Practice for Use of Langmuir Probes in Electric Propulsion Testing," *Journal of Propulsion and Power*, vol. 33, pp. 566–581, May 2017.

[21]K. Polzin, T. Markusic, B. Stanojev, A. Dehoyos, and B. Spaun, "Thrust stand for electric propulsion performance evaluation," *Review of Scientific Instruments*, vol. 77, 10 2006.

[22]M. Wijnen, J. Navarro-Cavalle, and P. Fajardo, "Mechanically Amplified Milli-Newton Thrust Balance for Direct Thrust Measurements of Electric Thrusters for Space Propulsion," *IEEE Transactions on Instrumentation and Measurement*, vol. 70, pp. 1–18, 2021.

[23]M. Wijnen, *Diagnostic Methods for the Characterization of a Helicon Plasma Thruster*. PhD thesis, Universidad Carlos III de Madrid, Leganés, Spain, 2022.

[24]M. R. Inchingolo, M. Merino, M. Wijnen, and J. Navarro-Cavalle, "Thrust measurement of a waveguide electron cyclotron resonance thruster," *Journal of Applied Physics*, 2024.

[25]H. Kim, Y. Lim, W. Choe, and J. Seon, "Effect of multiply charged ions on the performance and beam characteristics in annular and cylindrical type Hall thruster plasmas," *Applied Physics Letters*, vol. 105, p. 144104, Oct. 2014.

[26]H. Kim, W. Choe, Y. Lim, S. Lee, and S. Park, "Magnetic field configurations on thruster performance in accordance with ion beam characteristics in cylindrical Hall thruster plasmas," *Applied Physics Letters*, vol. 110, p. 114101, Mar. 2017.

[27]Y. Gao, H. Liu, P. Hu, H. Huang, and D. Yu, "The effect of magnetic field near the anode on cylindrical Hall thruster," *Plasma Sources Science and Technology*, vol. 25, p. 035011, June 2016.

[28]J. Gayoso, Y. Raitses, and N. Fisch, "Cathode Effects on Operation and Plasma Plume of the Permanent Magnet Cylindrical Hall Thruster," in *47th AIAA/ASME/SAE/ASEE Joint Propulsion Conference & Exhibit*, (San Diego, California), American Institute of Aeronautics and Astronautics, July 2011.